JOURNAL OF VIROLOGY, Feb. 2008, p. 1414–1424 Vol. 82, No. 3
0022-538X/08/$08.00+0 doi:10.1128/JVI.01674-07

Amino Acid Substitutions in the S2 Subunit of Mouse Hepatitis Virus Variant V51 Encode Determinants of Host Range Expansion▽

Willie C. McRoy[1]† and Ralph S. Baric[1,2]*

Department of Microbiology and Immunology, School of Medicine, University of North Carolina at Chapel Hill, Chapel Hill, North Carolina 27599-7290,[1] and Department of Epidemiology, School of Public Health, University of North Carolina at Chapel Hill, Chapel Hill, North Carolina 27599-7435[2]

Received 1 August 2007/Accepted 12 November 2007

We previously described mouse hepatitis virus (MHV) variant V51 derived from a persistent infection of murine DBT cells with an expanded host range (R. S. Baric, E. Sullivan, L. Hensley, B. Yount, and W. Chen, J. Virol. 73:638–649, 1999). Sequencing of the V51 spike gene, the mediator of virus entry, revealed 13 amino acid substitutions relative to the originating MHV A59 strain. Seven substitutions were located in the amino-terminal S1 cleavage subunit, and six were located in the carboxy-terminal S2 cleavage subunit. Using targeted RNA recombination, we constructed a panel of recombinant viruses to map the mediators of host range to the six substitutions in S2, with a subgroup of four changes of particular interest. This subgroup maps to two previously identified domains within S2, a putative fusion peptide and a heptad repeat, both conserved features of class I fusion proteins. In addition to an altered host range, V51 displayed altered utilization of CEACAM1a, the high-affinity receptor for A59. Interestingly, a recombinant with S1 from A59 and S2 from V51 was severely debilitated in its ability to productively infect cells via CEACAM1a, while the inverse recombinant was not. This result suggests that the S2 substitutions exert powerful effects on the fusion trigger that normally passes from S1 to S2. These novel findings play against the existing data that suggest that MHV host range determinants are located in the S1 subunit, which harbors the receptor binding domain, or involve coordinating changes in both S1 and S2. Mounting evidence also suggests that the class I fusion mechanism may possess some innate plasticity that regulates viral host range.

The cross-species transmission of human immunodeficiency virus (HIV) from chimpanzees and severe acute respiratory syndrome coronavirus (SARS-CoV) from bats and civet cats are salient examples of zoonotic transmission into the human population (28, 30, 36, 37). Surveys of all known human pathogens document this spillover, most recently noting that 58% are zoonotic in origin, with 73% of these zoonotic pathogens considered emerging or reemerging (59, 66). Viruses, particularly RNA viruses, are well represented among emerging pathogens (65, 67). The expansion of viruses into new hosts remains a poorly understood process. The CoV mouse hepatitis virus (MHV), the prototype member and molecular model for the genus, was utilized to study mechanisms of host range expansion. Two models for host range expansion were established; the first was based on a persistent infection scenario, while the second modeled a coinfection in a mixed host cell environment (3, 4). Variants derived from these model systems possessed an extended host range that included normally MHV nonpermissive hamster, monkey, feline, and human cell lines. The utility of these model systems has been exploited elsewhere, with a similar persistent infection system also used by Schickli et al. to generate MHV host range variants (53).

The genus *Coronavirus* includes a diverse membership of enveloped, single-stranded, positive-sense RNA viruses, historically divided into three groups (I, II, and III) based on immunological characteristics. CoVs infect a diverse repertoire of hosts, including turkeys, cats, cattle, dogs, and humans. The prototype group II member MHV naturally infects mice to induce enteric or central nervous system disease, depending on the strain. CoVs in general and MHV in particular are regarded as species specific, limited by availability of the appropriate cellular receptor to initiate infection (10, 15, 19, 21, 61, 70). The exception for MHV appears to be the neurotropic JHM strain that has been shown in a primate model to infect the central nervous system and also a human hepatocarcinoma cell line (11, 32, 45). MHV binds CEACAM1 on the cell surface to initiate infection (6, 13, 20, 46, 71). While virus affinity for CEACAM1 and its assortment of alleles and isoforms varies, CEACAM1a appears to have the highest affinity with all described MHV strains capable of initiating infection via this receptor. CEACAMs are conserved across mammalian genomes to include multiple representatives in the human genome (5).

The binding of MHV to its receptor is accomplished via the envelope-anchored spike (S) glycoprotein (Fig. 1). Spike is a class I fusion protein translated initially as a single large 180-kDa protein that is subsequently cleaved by a cellular protease into two noncovalently associated 90-kDa subunits, the amino-terminal S1 subunit and carboxy-terminal S2 subunit (9, 42). A putative receptor binding domain (RBD) has been mapped to the first 330 amino acids of S1 and primarily determines receptor specificity (33, 62). S2 contains the transmembrane domain and two heptad repeat regions (HR1 and HR2) (7, 9, 16, 68). Heptad repeats are conserved features of class I fusion

* Corresponding author. Mailing address: University of North Carolina at Chapel Hill, 2107 McGavran Greenberg Hall, CB 7435, Chapel Hill, NC 27599-7435. Phone: (919) 966-3895. Fax: (919) 966-0584. E-mail: rbaric@email.unc.edu.

† Present address: Mount Marty College, 1105 West 8th Street, Yankton, SD 57078.

▽ Published ahead of print on 21 November 2007.

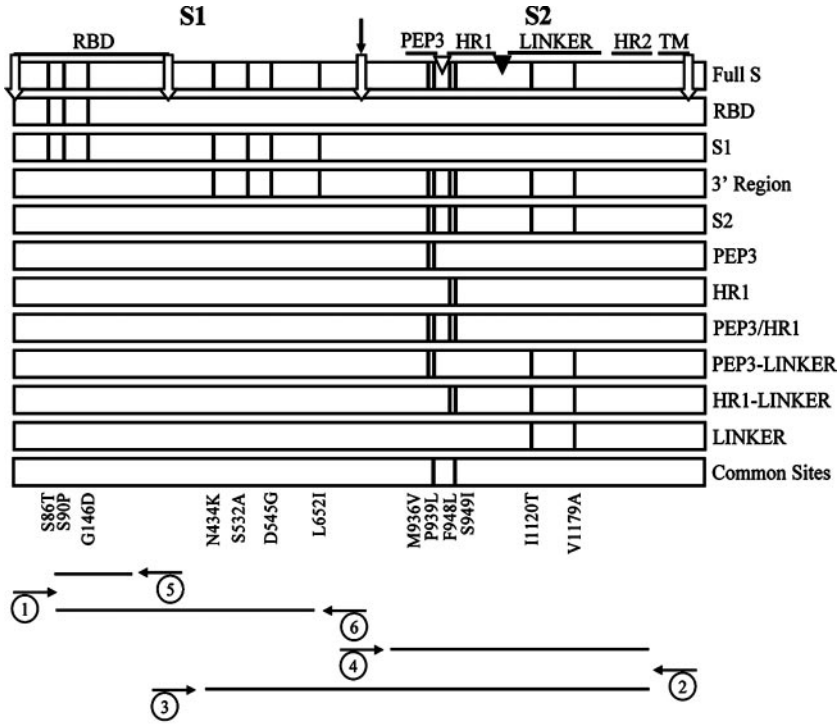

Primer	Sequence
1	NNNNNNCGTCTCGATTGCATGAGGCATAATCTAAAC
2	NNNNNNCGTCTCTGTCCTCCATACTCATCACAACA
3	NNNNNNCGTCTCGAGGAGTGGCTTACTGCTAGGTC
4	NNNNNNCGTCTCTCTACTGGCTATCGGTTAACTACATTTG
5	NNNNNNCGTCTCCTCCTCTATATTACAAGCTGGGAGG
6	NNNNNNCGTCTCAGTAGAAACTGATCGGTGAGCCC

FIG. 1. Spike protein structure map and cloning strategy. The panel of 12 chimeric S genes produced for this study is depicted, with the approximate locations of substitutions present in V51 relative to the A59 strain indicated as vertical black bars (numerical locations are indicated along the bottom of the figure). The 1,324-residue spike protein is typically posttranslationally cleaved between residues 717 and 718 into S1 and S2 subunits (cleavage site indicated with black arrow). The locations of characterized functional domains are indicated with black bars. The amino-terminal 330 residues of S1 comprise the RBD. S2 includes the putative fusion peptide PEP3 (residues 929 to 944), HR1 (residues 947 to 1048), a linker region (residues 1049 to 1214), HR2 (residues 1215 to 1262), and a transmembrane domain (TM) (residues 1264 to 1286). The four principal PCR products generated to facilitate chimeric S gene construction are indicated flanked by the corresponding primers. Primer 1 is the forward primer for both products in the S1 region, while primer 2 is the reverse primer for both products in the S2 region. Primer sequences are provided, and the locations of engineered No See'm sites are marked with open arrows. Randomized nucleotides (N′s in the sequences) were incorporated during primer synthesis to increase BsmbI restriction digest yields. Naturally occurring AlwNI (open triangle) and MluI (filled triangle) restriction sites within S2 were used in conjunction with the engineered No See'm sites to subdivide the substitutions present in this region.

proteins that form the classic six-helix bundle believed to drive virion-cell membrane fusion (14, 23). Several candidate fusion peptides have been identified in S2, but none have conclusively been demonstrated as fulfilling this role in MHV (12, 41). Current evidence supports an infection model initiated with S1 engaging the cell surface receptor, thereby triggering a conformational change in S2, leading to the fusion of the viral envelope and cell membrane (26, 44, 56, 64, 74).

We previously described variant V51 with an expanded host range phenotype to include cell lines from MHV nonpermissive species (3). V51 was derived from a persistent infection of murine DBT cells, with the infection initiated by the hepatotropic MHV prototype strain A59. Mutations responsible for this expansion of host range developed between 119 and 210 days postinfection and conferred on V51 the ability to recognize an assortment of human CEACAMs as receptors. Human CEACAM usage within a given cell line was diverse and not attributable to a single receptor allele, suggesting that additional elements were associated with V51 host range expansion. The goal of this study was to isolate the genetic determinants in S mediating the expanded host range phenotype of V51.

MATERIALS AND METHODS

Cell lines and viruses. Murine DBT cells were maintained in minimum essential medium (MEM) supplemented with 6% fetal clone II (FCII) (HyClone), 5% tryptose phosphate broth (Sigma), and 1% gentamicin-kanamycin. Human HepG2 cells were maintained in MEM supplemented with 10% FCII, 0.1 mM nonessential amino acids (NEAA), and 0.1 mM sodium pyruvate. Feline AKD cells were maintained in Ham's F12K (Kaighn's modification) and 10% FCII. Chinese hamster ovary K1 and pgsA-745 cells (ATCC no. CRL-2242) were maintained in MEM, 10% FCII, and 0.1 mM NEAA. Human MCF7 cells were maintained in Dulbecco's modified Eagle medium supplemented with 0.1 mM NEAA, 10% FCII, and 0.01 mg/ml insulin. Swine testicular (ST) cells stably expressing murine CEACAM1a were produced by using CEACAM1a under the

control of a cytomegalovirus promoter in the pcDNA3 vector (kindly provided by Kathryn Holmes). ST cells were transfected by using calcium phosphate and stably expressing cells isolated via Geneticin selection, followed by two rounds of sorting for CEACAM1a expression (29). ST-CEACAM1a-expressing cells were maintained in MEM, 10% FCII, 0.1 mM NEAA, 0.1 mM sodium pyruvate, 0.005 g/ml lactoalbumin, and 1 mg/ml Geneticin. All cells were cultured at 37°C and 5% CO_2.

MHV variant V51 was isolated previously (3). MHV A59 was produced via targeted RNA recombination by using the pMH54 vector (34). Feline MHV (fMHV) used in targeted recombination was supplied by Paul Masters, and working stocks were produced with AKD cells.

S gene isolation and recombinant virus construction. The S gene from the original V51 host range mutant was isolated from viral RNA by using SuperScript II reverse transcriptase (Invitrogen), followed by PCR amplification (Expand Long Template PCR system; Roche) with the approximately 4-kb product ligated into the TOPO-XL vector (Invitrogen). Multiple clones were selected and sequenced to create a consensus spike gene sequence from which all recombinants in this study were developed. The strategy, which was used to produce recombinant viruses with only the desired mutations, is outlined in Fig. 1. S gene regions encoding the RBD, the S1 cleavage subunit, the S2 cleavage subunit, and all of S, excluding the receptor binding domain (3′ region), were PCR amplified from either the V51 consensus spike or the MHV A59 donor plasmid pMH54 (kindly provided by Paul Masters) by using primers incorporating terminal No See'm sites (BsmBI restriction sites) to allow for the seamless joining of PCR products (34, 72). The six mutations in the S2 portion of S were subdivided by taking advantage of unique AlwNI and MluI restriction sites present in both the V51 and MHV A59 S genes in conjunction with the introduced BsmBI sites. The chimeric S genes produced by combining V51 and MHV A59 pieces were then cloned into a modified pMH54 targeting vector (pMH54mod) for the production of virus.

pMH54mod was engineered by first removing the wild-type MHV A59 S gene from pMH54 via unique Eco47III and EagI sites in the hemagglutinin esterase and matrix genes, respectively. This approximately 5.5-kb restricted fragment was replaced with a PCR product derived from pMH54 engineered to incorporate BsmBI sites corresponding to terminal chimeric S gene BsmBI sites (Fig. 1) to facilitate cloning. Primer HEICA59 (5′-CATTCCAAGGGCAGCTCTTC-3′) was paired with RSR2BSMB (5′-TGACGGACCGAGTCACGTCTCGCAATC TAACACCGCTATCCGTC-3′) to produce a PCR product spanning from the Eco47III site to 19 nucleotides upstream of the ATG start in S. The primer RSR2ESP (5′-ACTCGGTCCGTCAGTCGTCTCAGGACACCAGGACAGT ATTGTG-3′) was paired with MREVA59 (5′-AATGCCCAACGAGAAGTTC C-3′) to produce a PCR product spanning from 47 nucleotides upstream of the S TGA stop codon to the EagI site. These two PCR products were then restricted with RsrII (engineered into the above primers along with the BsmBI sites) to facilitate their ligation, followed by Eco47III and EagI restriction for ligation into the spot vacated by the original 5.5-kb restriction fragment producing pMH54mod. All chimeric S genes begin with the ATG start of S and end 47 nucleotides upstream of the TGA S stop codon. No mutations were present in the 3′ 47 nucleotides of S; hence, this sequence was preserved in the pMH54mod vector. The common sites recombinant that incorporated mutations common to other MHV host range model systems (positions 939 and 949) required primer-introduced mutations using primers HSREV (5′-CAGCAGCTGCCGGTGTG CCATTTATTTTAAGCG-3′) and HSFWD (5′-CAGCTGCTGACCACAGTG GGAACATAGC-3′) in conjunction with the AlwNI and BsmBI sites.

The details of the fMHV-targeted RNA recombination system are well established (34); however, the conditions used in this study are slightly altered. Briefly, subconfluent monolayers of feline AKD cells were infected with donor virus fMHV for 1 h at 25°C and then medium was added and the cells were incubated at 37°C for 4 h. The infected AKD cells were then trypsinized, washed, and resuspended in cold phosphate-buffered saline (PBS). pMH54mod plasmids containing A59/V51 chimeric S genes were PacI digested to produce linearized templates for transcription by using a T7-based system (mMessage mMachine; Ambion) following the manufacturer's instructions. Transcripts were mixed with the cells, followed by two electroporation pulses at 50 uF and 0.3 kV (GenePulser XCell; Bio-Rad). Electroporated cells were then overlaid onto subconfluent layers of murine DBT cells to select for recombinants. Twenty-four to 36 h postelectroporation, the medium was harvested and frozen. This medium was used as a starting point for two rounds of plaque purification per recombinant. Following the second round of purification, recombinant viral RNA was collected and the S gene reverse transcription-PCR product cloned and sequenced to verify the presence of the desired S gene mutations. Electroporations were performed in duplicate for each construct to minimize potentially advantageous mutations arising in the genome outside the S gene. Twice-plaque-purified and S gene-sequence-verified viruses were then expanded for use in experiments.

TABLE 1. Substitutions in spike proteins arising during a persistent infection

Virus	Spike protein position by residue												
	S1							S2					
	86	90	146	434	532	545	652	936	939	948	949	1120	1179
A59	S	S	G	N	S	D	L	M	P	F	S	I	V
V8	S	S	D	N	A	D	I	M	P	F	S	T	V
V19	S	S	G	N	A	D	I	M	P	F	I	T	V
V30	S	S	G	N	A	D	I	M	P	F	S	T	V
V51	T	P	D	K	A	G	I	V	L	L	I	T	A

Growth curve analysis. Eight-well chamber slides (Labtek) or 96-well tissue culture plates (Corning) were seeded with the desired cell type (HepG2, MCF7, etc.), and the cells were allowed to regain typical morphology prior to infection. Cells were infected at a fixed multiplicity of infection (MOI) (the MOI was 5 unless explicitly stated otherwise) for 1 h at 25°C and then washed with PBS to remove unbound virus prior to the addition of medium. Titers at various time points were determined via plaque assay with DBT cells as described previously (2). Briefly, 10-fold serial dilutions of virus were inoculated onto confluent DBT cells for 1 h at 25°C and then the monolayers were overlaid with 0.8% agarose medium. Plaques were visualized 48-h postinfection by neutral red staining and enumerated.

Immunofluorescence staining. Chamber slides were seeded with the desired cell type, and the cells were allowed to regain typical morphology. Cells were infected at an MOI of 5 for 1 h at room temperature and then washed with PBS to remove unbound virus prior to the addition of medium. At 36 h postinfection, slides were fixed in 50:50 methanol-acetone at −20°C for at least 12 h. Fixed slides were rehydrated for 10 min in PBS and then stained with an anti-nucleocapsid protein monoclonal antibody (kindly provided by Julian Liebowitz) for 2 h at room temperature. The primary antibody was washed off and followed with fluorescein isothiocyanate-conjugated anti-mouse secondary antibody for a half hour at room temperature. After further washing, coverslips were mounted using 80:20 glycerol-water. Photos were taken with an Olympus IX51 microscope and a Hamamatsu camera controlled by IP Lab software, version 3.5.

Receptor blockade assay. ST-CEACAM1a cells stably expressing CEACAM1a [1-4] or DBT cells were seeded in chamber slides or 96-well plates as described above. Anti-CEACAM1a monoclonal antibody CC1 (kindly provided by Kathryn Holmes) was added to monolayers at 0.05 mg/ml in cell medium for 30 min at 37°C prior to infection (22). Cells were then infected following the growth curve protocol described above, except that the medium added after washing unbound virus contained CC1 or an isotype-matched control antibody (22).

RESULTS

Sequence analysis of host range mutants. It has been well established that receptor binding and cellular entry, functions of the S protein, determine cellular susceptibilities to MHV and other CoV infections (10, 19, 21). Given this gatekeeper function, the S genes from a temporal series of variants leading to V51 (V8, V19, and V30) were individually PCR amplified, cloned, and sequenced to develop consensus genes at each time point (3). V8 was isolated 30 days post-initial A59 infection, V19 was isolated at 75 days post-initial A59 infection, and V30 was isolated at 119 days post-initial A59 infection. Sequencing revealed the presence of 13 amino acid changes in V51 relative to the reference A59 strain used in the targeted RNA recombination system (Table 1). Seven substitutions (S86T, S90P, G146D, N434K, S532A, D545G, and L652I) were located in the S1 subunit, with three residing in the RBD. The remaining six substitutions (M936V, P939L, F948L, S949I, I1120T, and V1179A) were in S2. Three substitutions (S532A, L652I, and I1120T) occurred early in variant V8 isolated at 30

TABLE 2. Common substitution sites in S among MHV host range models

Virus	S protein position by residue			
	936	939	949	1120
A59	M	P	S	I
pi23[a]	M	P	R	I
pi600[a]	L	P	R	T
MHV/BHK[a]	L	P	R	T
V51	V	L	I	T
C4[b]	M	ΔP	R	T

[a] Reference 52.
[b] Unpublished data.

days postinfection and were retained throughout the remaining 180 days of infection leading to V51. Substitutions G146D and S949I are present in early isolates V8 and V19, respectively, and then they disappear from later-sequenced isolates, only to reappear in V51. As previously reported, the substitutions mediating V51 host range expansion evolved most clearly between 119 and 210 days post-initial inoculation, corresponding to variants V30 and V51, respectively (3). This result also represents the greatest gain in substitutions from one variant to the next. A second V51 isolate (V51A) from the persistent infection model was also cloned and sequenced to develop a consensus S gene. There are four additional substitutions in V51A relative to A59 and V51: W259G, S537P, L1102F, and V1226I (data not shown). V51 was selected over V51A for further characterization for simplicity, as the altered host range phenotypes of both isolates were similar (3).

Two additional MHV-based systems examining host range have previously been reported. Variants pi23, pi600, and MHV/BHK were derived from a similar persistent infection model of murine 17Cl1 cells, while MHV-C4 was derived from a coinfection of MHV strains JHM and A59 in a mixed-cell environment of both murine and hamster cells (4, 52, 53). Comparing the S protein sequences from these variants reveals four sites of commonality (Table 2). At position 1120, V51 shares a common isoleucine-to-threonine change with MHV/BHK and pi600 (C4 also encodes a threonine; however, a threonine at this position is also present in the parental JHM strain). A second change at M936 results in leucines in MHV/BHK and pi600, while V51 encodes a valine. At position 939, V51 encodes a leucine in place of proline, while this codon is deleted in C4. A substitution at site S949 is common to all three systems. V51 encodes an isoleucine at position 949, while C4, MHV/BHK, pi23, and pi600 share an arginine. Position 1120 is located in the linker region between HR1 and HR2. Positions 936 and 939 are located in a region previously identified as PEP3, a putative fusion peptide (12). Position 949 is potentially the most interesting change due to its presence in all three systems, its location in HR1, and its close proximity to substitutions at positions 936, 939, and 948 in V51.

Mapping determinants of host range. The critical role of S in initiating infection has led to the identification of several of its important regions that are responsible for receptor binding and subsequent virion-cell membrane fusion (Fig. 1). Recombinant viruses containing only the desired combination of S gene mutations were generated by using the fMHV-targeted RNA recombination system, No See'm technology, and naturally occurring restriction sites (34, 72). A panel of 12 recombinant viruses was produced to facilitate mapping host range determinants (Fig. 1). Each recombinant focused on the changes in V51 located in the recognized functional regions or dissected the clustered changes in S2. A single recombinant, common sites recombinant, focused on the P939 and S949 changes found in host range variants from other model systems. V51 recombinants produced plaques approximately one quarter the size of A59 by 48 h postinfection, but plaque margins were well defined in a manner similar to those of A59 (data not shown).

V51, but not A59, displayed robust replication in the human hepatocarcinoma cell line HepG2 despite no previous exposure during isolation (3). Thus, subsequent growth curve analysis and mapping of recombinants were performed primarily in this cell line. Growth curve analysis was selected as the primary assay as this represents a more stringent measure, in our opinion, of the impact on host range of given changes since it relies on the formation and recovery of a functional virion.

Given the critical role of receptor binding in determining cellular entry and the reports implicating changes in S1 as contributing to broad alterations in host range, the Full S, S1, and RBD recombinants were initially produced and evaluated to assess the contribution of substitutions in these functional regions (17, 52, 60). By 48 h postinfection, the S1 and RBD recombinants replicated to titers approximately 3 logs lower ($<1 \times 10^4$ PFU/ml) than those of either the Full S recombinant (8.8×10^6 PFU/ml) or V51 (1.3×10^7 PFU/ml) and comparable to those of the A59 background (Fig. 2A). The robustness of the Full S recombinant relative to V51 suggests that important host range determinants are indeed located in S; however, the involvement of other genes in determining host range cannot be excluded. The unexpectedly low titers from the RBD and S1 recombinants prompted us to construct the S2 and 3′ region recombinants. The S2 and 3′ region recombinants yielded titers on par with that of V51 by 48 h postinfection (Fig. 2B). V51 replicated to 3.35×10^6 PFU/ml, while the S2 recombinant peaked at 5.35×10^6 PFU/ml and the 3′ region recombinant peaked at 1.35×10^7 PFU/ml. The robust replication of both the 3′ region and S2 recombinants suggests that important determinants of host range are located exclusively in S2, a phenomenon not documented previously with CoVs. The growth curves presented in Fig. 2A and B are representative of multiple independent experiments that were performed to minimize the variability of HepG2 cell clumping during the seeding process, rather than relying on a single growth curve repeated in triplicate. Average 48-h titers for the five recombinant viruses reinforced the results that S2 alone can encode determinants of MHV host range. As shown in Fig. 2C, the average 48-h titer for V51 was 9.15×10^6 PFU/ml, while those of the Full S, S2, and 3′ region recombinants were comparable at 5.19×10^6, 8.58×10^6, and 1.78×10^7 PFU/ml, respectively. These average titers were all well over 400 times those of the RBD and S1 recombinants (3.92×10^3 and 1.09×10^4 PFU/ml, respectively), which were more comparable to the A59 background level of 2×10^3 PFU/ml.

The novelty of host range determinants exclusively in S2 prompted a more detailed analysis of the substitutions in this subunit. As previously discussed, four of the six S2 substitutions reside in regions characterized experimentally, the PEP3

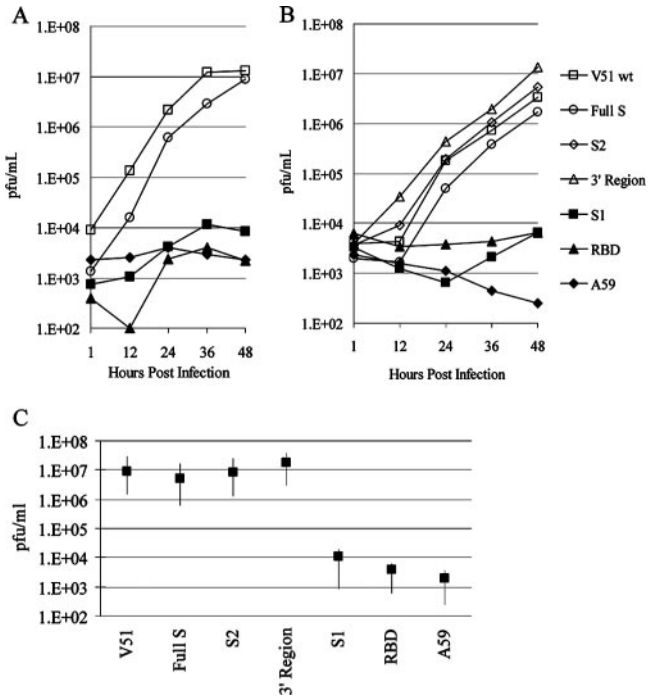

FIG. 2. Mapping of host range determinants on human HepG2 cells. Monolayers of HepG2 cells were infected at an MOI of 5, and virus titers at indicated time points were determined via plaque assay with murine DBT cells. (A and B) Representative growth curves reported as PFU per milliliter. Data points are identified by the key provided on the far right. (C) Average titers of recombinants across multiple growth curves. The black squares indicate the average titers, while the arms signify the maximum and minimum titers recorded per recombinant across a minimum of four growth curves.

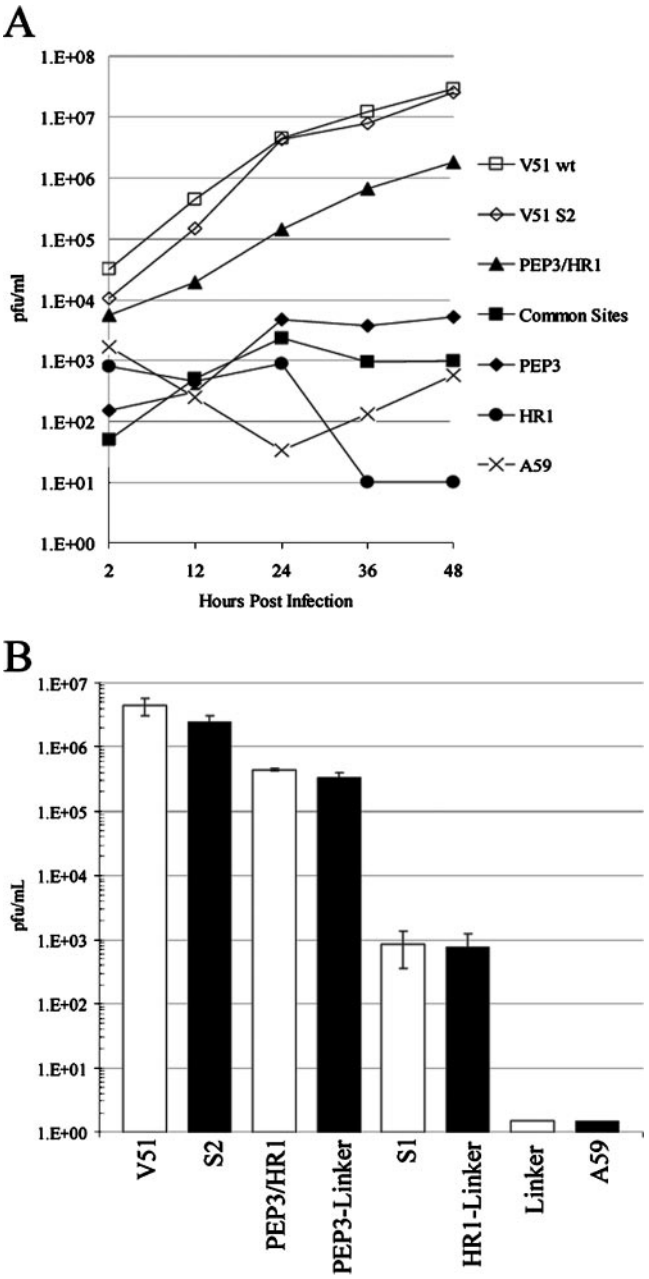

FIG. 3. Mapping of host range determinants within the S2 subunit. Monolayers of HepG2 cells were infected at an MOI of 5, and virus titers at indicated time points were determined via plaque assay with murine DBT cells. (A) Representative growth curve dissecting the contributions of substitutions in the PEP3 and HR1 domains on host range. (B) Titers for HepG2 cells at 48-h postinfection, focusing on S2 substitutions in combinations. Infections per recombinant were performed in triplicate, with error bars (standard deviations) indicated.

putative fusion peptide (41) and HR1 (9, 16) (Fig. 1). Preserving the substitutions in PEP3 and HR1 as an intact unit in the PEP3/HR1 recombinant provided a 48-h postinfection titer for HepG2 cells of 1.79×10^6 PFU/ml (Fig. 3A). This titer was about 10-fold lower than those of V51 and the S2 recombinant (2.9×10^7 and 2.52×10^7 PFU/ml, respectively). The PEP3 and HR1 recombinants divide this four-substitution unit into the separate functional regions. Forty-eight-hour titers for either recombinant were about 2 logs or more lower than the titers determined when the substitutions are preserved as a unit, although the PEP3 recombinant was more robust at 5.3×10^3 PFU/ml than was the HR1 recombinant at 10 PFU/ml. The 939L and 949I mutations in PEP3 and HR1 that are common to other host range model systems mentioned previously (see "Sequence analysis of host range mutants" above) were incorporated into the common sites recombinant. It replicated to 9.7×10^2 PFU/ml by 48 h postinfection, comparable to the A59 background level of 5.7×10^2 PFU/ml (Fig. 3A).

The potential contribution of the 1120T and 1179A substitutions located in the linker region between HR1 and HR2 (Fig. 1) prompted the construction of three additional recombinants that paired the PEP3 or HR1 substitutions with 1120T and 1179A (PEP3-linker recombinant and HR1-linker recombinant, respectively) or the 1120T and 1179A substitutions alone (linker recombinant). By 48 h, the HR1-linker recombinant titer was 7.7×10^2 PFU/ml, over 2 logs below the titer for PEP3/HR1 at 4.43×10^5 PFU/ml (Fig. 3B). The PEP3-linker recombinant titer of 3.3×10^5 PFU/ml was comparable to the PEP3/HR1 recombinant titer of 4.43×10^5 PFU/ml. Replication of the linker recombinant at 48 h was virtually undetectable by plaque assay. While not as robust a phenotype as the S2 recombinant with all six substitutions (2.5×10^6 PFU/ml), it is clear that coordinating mutations in PEP3, HR1, and the

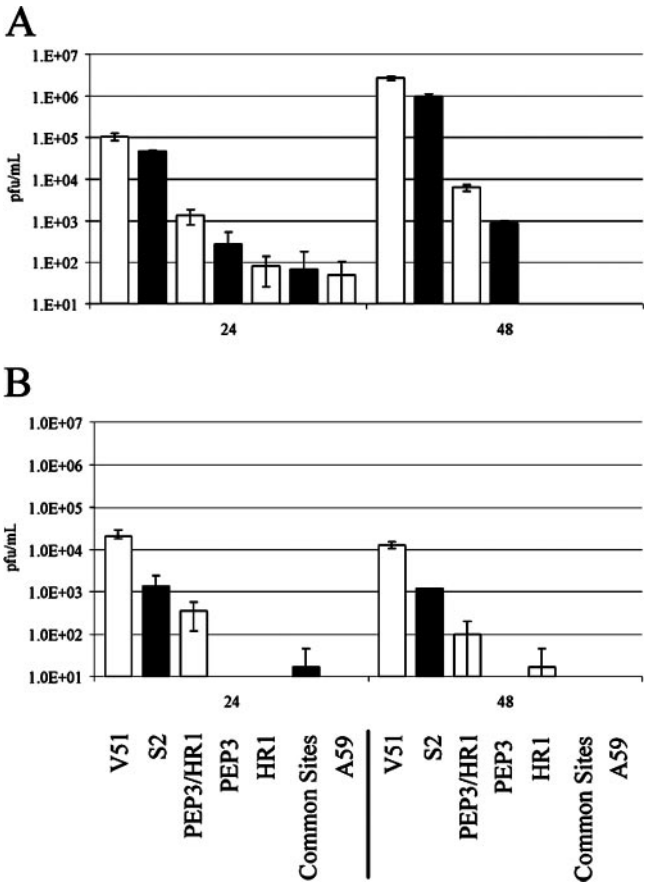

FIG. 4. Recombinant virus replication in CHO and MCF7 cells. Monolayers of cells were infected at an MOI of 5 in triplicate, and titers at 24 and 48 h were determined by plaque assay with DBT cells. Infections per recombinant were performed in triplicate, with error bars (standard deviations) indicated. The bar labels at the bottom apply to both panels. (A) Hamster CHO cells. (B) Human MCF7 cells.

linker region are important mediators of V51 host range expansion.

We previously reported that V51 could also replicate in Chinese hamster ovary (CHO) and human breast carcinoma (MCF7) cells (3). To determine whether the S2 substitutions important in HepG2 entry represent more generalized mediators of entry into normally nonpermissive cell lines, 24- and 48-h titers were also measured for these cell lines. In CHO cells, the S2 substitutions were also important host range mediators, as the 48-h peak titer for the S2 recombinant was 9.65×10^5 PFU/ml, comparable to the V51 titer of 2.7×10^6 PFU/ml (Fig. 4A). This result suggests that the S2 substitutions are not specific for entry into HepG2 cells. When we subdivided the S2 mutations, the PEP3/HR1 recombinant replicated to 6.3×10^3 PFU/ml by 48 h postinfection, about 2 logs below the value for the S2 recombinant, but 1,000-fold higher than the values for HR1 and common sites recombinants or A59 (all three of which were not detected via plaque assay at 48 h). MCF7 cells are permissive to initial infection by V51 and the S2 and PEP3/HR1 recombinants; however, the infection appears to stall and titers decline by 48 h (Fig. 4B).

Immunofluorescence analysis of infected cells. Despite the evidence that MHV infection is regulated at the level of receptor binding and entry, we were concerned about a possible block at a postentry stage that did not allow for the recovery of some recombinants from cells (i.e., assembled virus was retained in the cells). To verify that recombinants incapable of productively replicating in HepG2 cells were blocked at cellular entry, monolayers infected with a subset of the recombinant virus panel were immunolabeled with an anti-nucleocapsid protein monoclonal antibody. Reflecting the growth curve data, the Full S, S2, 3′ region, and PEP3/HR1 recombinants all displayed qualitatively strong but varying degrees of nucleocapsid staining similar to that with V51 (Fig. 5). This result was in marked contrast to the result for recombinants unable to replicate above A59 background levels in HepG2 cells as assessed by plaque assay. By immunofluorescence, only a rare stained cell could be located in the monolayers for the RBD,

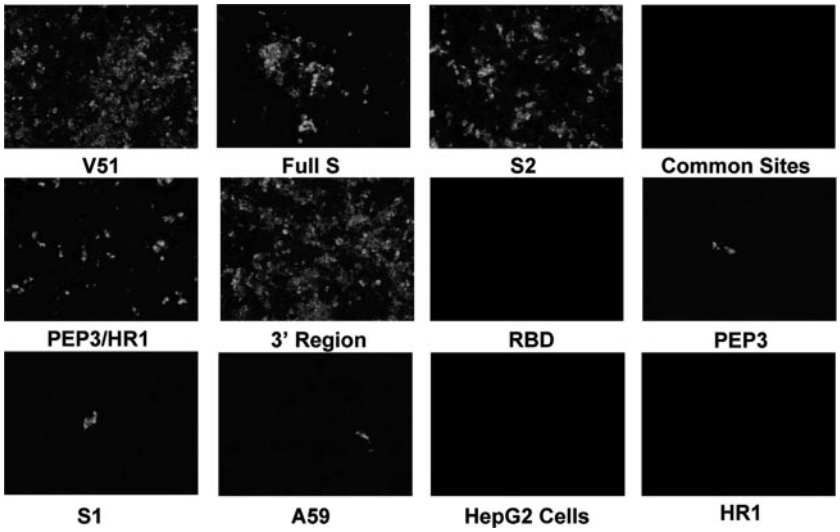

FIG. 5. Immunofluorescence analysis of HepG2 cells. Monolayers of HepG2 cells infected at an MOI of 5 were fixed and stained with anti-N protein monoclonal antibody. Photos are representative fields for each recombinant.

S1, PEP3, HR1, and common sites recombinants, a pattern seen with A59 as well. The staining pattern mirrors the plaque assay data in other cell types, such as CHO cells, again suggesting that a block at entry is responsible for the lack of recovery of some recombinant viruses (data not shown).

Receptor usage. We previously reported that V51 had broadened its receptor affinity such that it could utilize human CEACAMs to initiate infection (3). Given that changes facilitating host range expansion were mapped to the S2 subunit and not the RBD or S1, we explored the recognition of the high-affinity MHV receptor CEACAM1a with select members of our recombinant panel. ST cells are normally nonpermissive to MHV infection by either A59 or V51 (titers at time zero were approximately 2×10^4 to 4×10^4 PFU/ml, decreasing at 30 h postinfection to 1×10^2 or 7.4×10^2 PFU/ml, respectively) (3, 4). A similar nonpermissive phenotype was seen following V8, V19, and V30 virus infection as well (data not shown). To overcome this barrier, ST cells were modified to stably express the murine CEACAM1a receptor from a plasmid (ST-CEACAM1a) (29). ST-CEACAM1a cells were inoculated with V51, and select recombinants were then used to analyze receptor usage. V51 and the Full S and S2 recombinants (2.2×10^4, 9.8×10^2, and 7.1×10^3 PFU/ml, respectively) replicated to titers 150-fold below those of A59 and the S1 recombinant (8.1×10^6 and 3.7×10^6 PFU/ml, respectively) (Fig. 6A). Both V51 and the S1 recombinant share the seven substitutions in the S1 subunit, but these changes do not permit robust ST-CEACAM1a-mediated infection in the context of V51 or the Full S recombinant. S1 recombinant replication is comparable to that for A59, suggesting that substitutions in S1 do not radically affect the ability of the V51 RBD to recognize CEACAM1a. Interestingly, the S2 recombinant titers lagged behind those of A59, despite possessing S1 from A59. Viral replication titers qualitatively correlated with results of anti-nucleocapsid protein immunofluorescence analysis of infected ST-CEACAM1a cells, where nucleocapsid-positive cells were readily detected with A59 and the S1 recombinant, but not with V51 or the Full S and S2 recombinants (data not shown).

The monoclonal antibody CC1 likely prevents A59 infection by specifically binding to a location on CEACAM1a that overlaps with the A59 binding site, thus blocking viral access to the receptor (22, 55). Pretreatment of ST-CEACAM1a cells with CC1 effectively inhibits infection by A59 and the S1 recombinant, dropping 24-h titers 100,000-fold or more (Fig. 6A). The effect of CC1 on the limited replication of V51 and the full S and S2 recombinants was minor, about 70-fold at maximum for V51. Isotype-matched control antibodies did not specifically reduce titers (data not shown). On DBT cells, CC1 blockade of CEACAM1a again reduces A59 and S1 recombinant titers by 50,000- and 5,000-fold, respectively (Fig. 6B). V51 and the S2 and Full S recombinants are more resistant to CC1 blockade, dropping titers only 20-fold at maximum for the Full S recombinant and much less for V51 and S2 recombinant. Taken together, the receptor blockade data suggest either that V51 and the S2-based recombinants recognize alternate receptors on permissive cells (DBT cells) or that the mutated S2 fusion domain allows for CEACAM1a-independent entry in multiple cell types (HepG2, MCF7, and CHO cells).

Previous studies have demonstrated that tissue culture adaptation of viruses may result in the use of the ubiquitous proteoglycan heparan sulfate (HS) as a receptor or coreceptor, as demonstrated with Sindbis virus and the MHV/BHK variant (17, 31, 50). The mutations in V51 do not generate any HS binding sites (characterized by an XBBXBX motif) readily identifiable in the primary structure of the protein. The N434K

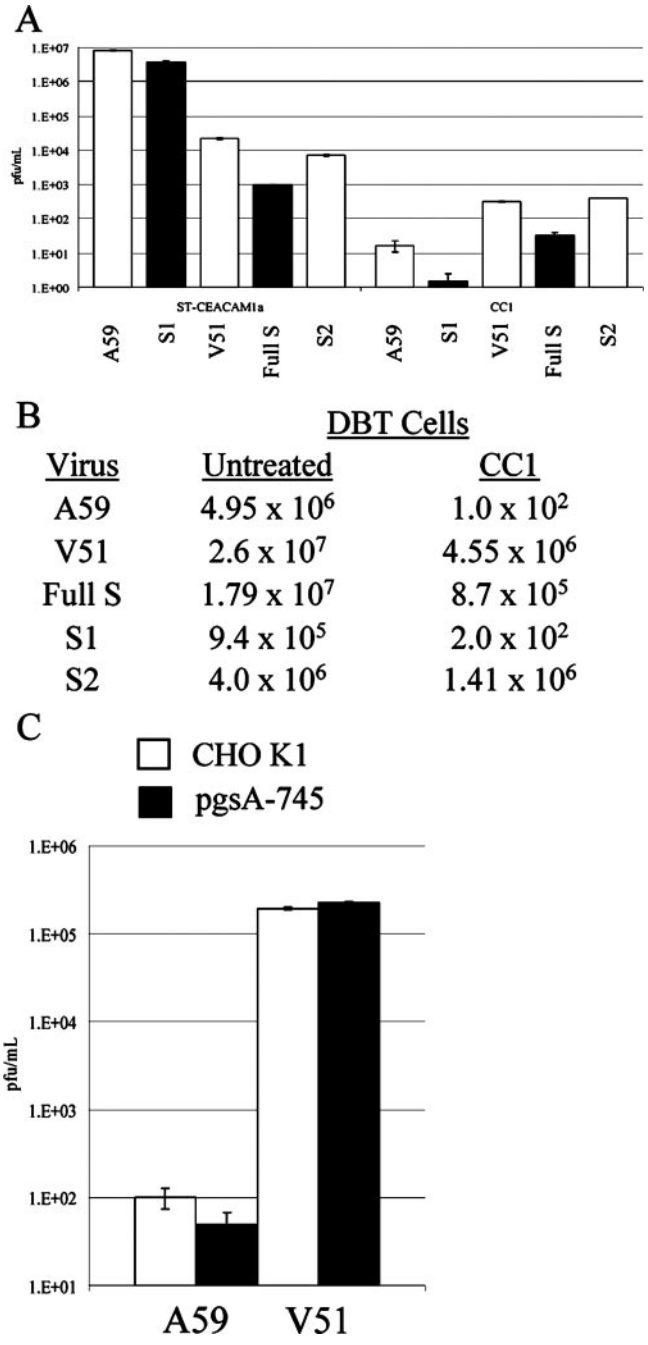

FIG. 6. Receptor utilization by recombinant viruses. Monolayers of ST-CEACAM1a, DBT, K1, or pgsA-745 cells were infected at an MOI of 5, and at 24 h postinfection, titers were determined via plaque assay on DBT cells. Infections were performed in triplicate, with error bars (standard deviations) indicated. (A) ST-CEACAM1a cells were untreated or pretreated with blocking antibody CC1. (B) DBT cells were untreated or pretreated with CC1. (C) HS-expressing CHO cells or nonexpressing pgsA-745 cells were infected with A59 or V51.

substitution is the only gain of a basic residue present, but the context of this change does not appear to form an HS consensus motif. To eliminate HS as a potential receptor for V51, CHO K1 cells expressing HS and pgsA-745 cells, CHO derivatives incapable of producing HS, were evaluated for V51 infection. At 48 h postinfection, titers averaged 1.9×10^5 and 2.3×10^5 PFU/ml on K1 and pgsA-745 cells, respectively ($P = 0.27$), suggesting a lack of HS involvement (Fig. 6C). A59 was unable to generate appreciable titers in either of these cell lines.

With the dramatic impact of the S2 substitutions, we were intrigued by the idea that S2 substitutions may facilitate receptor binding directly, thereby alleviating the need for the traditional RBD and CEACAM1a receptors for docking and entry. We designed a construct that deleted residues 21 to 560 of S1, while preserving the amino-terminal signal sequence, but were unable to recover virus with this deletion. S1 deletions are tolerated, particularly in JHM-derived strains, suggesting either that the deletion was too large to recover a functional S or that the RBD is still required for the entry of V51 (25).

DISCUSSION

The current working model for MHV entry into cells begins with the S1 subunit binding to a receptor, thereby inducing a conformational change in S2 that drives cell membrane-virion fusion (26). This model is analogous to that for other viruses possessing a class I fusion protein, such as HIV and influenza (23). Although a complete crystal structure for MHV spike is sorely missing, the structures for several distinct domains, including those of HR1 and HR2 in a presumed postfusion canonical six-helix bundle, have been solved (68). The mechanics of the trigger that drives the reorganization of S2 into this fusion core structure have yet to be determined, but experimental evidence points to regions in S1 interacting with S2 to drive this process.

Previously, mutations in the RBD and S1 have been identified as mediating host range expansion. Host range variant MHV/BHK was reportedly able to initiate low levels of entry into cell lines from several species, with the phenotype mapped to 21 substitutions and a unique 7-amino-acid insert in S1 despite the presence of 57 total substitutions in S (52, 53, 60). This mapping was limited to binding studies and replication in hamster cells, as the identified changes did not allow for progeny virion recovery or subsequent rounds of infection in nonmurine cells. The inability to produce secondary rounds of infection strongly suggests that an unknown number or combination of the remaining 36 amino acid changes scattered throughout S are vital to its extended host range phenotype. It was demonstrated more recently that during propagation, MHV/BHK acquired two new HS binding sites (one in S1 and the other in S2) and preserved a third at the S1-S2 cleavage site due to the apparent noncleavage of the S protein of this mutant (17). The presence of these sites, particularly the two newly acquired sites, bestowed upon MHV/BHK the ability to use HS as a receptor for entry into HeLa cells (18). The functionality of HS as a receptor in cells from additional species has not been reported, so it is unclear whether this is a HeLa cell-specific phenomenon or more broadly applicable to host range expansion.

Early studies in our laboratory showed that V51 infected BHK cells expressing high levels of human CEACAMs 1 and 5 (identified as BGP and CEA, respectively, under the previous nomenclature system) with low levels of efficiency, noting that many CEACAM 1- and 5-expressing cells were not productively infected. We concluded either that multiple combinations of CEACAM receptors functioned in docking and entry or that other mechanisms may help promote entry into human cells (3). In contrast to results for MHV/BHK and this earlier work, determinants of host range for V51 mapped exclusively to the S2 subunit, a phenomenon not previously documented for any CoV. The S2 changes also appear to represent a generalized alteration, facilitating entry into not only human cell lines but also those of hamster and monkey origin (data not shown). While the six substitutions in S2 were sufficient to mediate extended host range, the contribution of substitutions in S1 or elsewhere in the genome is also likely to be important for maintenance of the expansion, perhaps promoting higher-affinity interactions between the virus and cell surface to promote S2-driven entry. We have yet to examine potential genetic changes outside S, such as in the replicase genes or other structural proteins, that may be involved in V51 host range expansion. Experimental evidence from SARS-CoV suggests that alterations in its RBD were responsible for the initial host range jump; however, positive selection for mutations within the heptad repeats of S2 may have occurred once the virus entered the human population to refine the SARS-CoV interaction with the angiotensin-converting enzyme 2 receptor (24, 38, 75).

S2 has not been shown to possess inherent receptor binding activity (58), an observation supported by our lack of recovery of a recombinant that attempted to delete the RBD and additional S1 residues, although such a large deletion may sterically destroy the functionality of the remaining S glycoprotein. However, numerous studies have documented how substitutions in S2 alter properties of S1 and S as a whole, including stabilizing the S1-S2 association, altering fusion behavior, and changing tissue tropism (7, 18, 25, 27, 40, 43, 49, 51). Clearly, substitutions in S2, either alone or paired with corresponding substitutions in other regions of S, can have profound impacts upon the behavior of S, even leading to changes in host range. The coordination of S1 and S2 substitutions and their influence on host range was demonstrated recently with MHV/BHK entry into HeLa cells (18) and in our coinfection model (data not shown).

Most intriguing is the location of the identified substitutions in and adjacent to HR1, a conserved hallmark feature of class I viral fusion proteins. As previously mentioned, heptad repeat domains pack together to form the characteristic six-helix bundle believed to drive viral entry (14, 23). The M936V and P939L substitutions are both located adjacent to HR1 in PEP3, a region identified based on its hydrophobic composition as a potential fusion peptide (12, 41). The F948L and S949I substitutions are located at the amino-terminal end of HR1, as defined by Bosch et al., beginning with residue 947 (9).

The four clustered PEP3-HR1 substitutions all result in increasingly hydrophobic residues, an interesting feature relative to their locations in domains defined by such traits. The inclusion of these substitutions is not computationally predicted to extend the recognized helix of HR1 using the LearnCoil-VMF

program, an identifier of coiled-coil regions in viral fusion proteins (54). The presence of the four clustered substitutions at the amino terminus of HR1 is also interesting, as this area is not required for the formation of stable HR1-HR2 interactions, a key step in six-helix bundle construction in earlier studies (9, 68). Purified HR1 peptides used in one earlier study did not include the 948 and 949 residues of interest in V51; rather, they began at residue 953 and yet still complexed with HR2 (9). Additionally, a portion of the amino-terminal end of this HR1 peptide was susceptible to proteinase K degradation even when complexed with HR2, further suggesting a lack of involvement in interactions with HR2 in this system. A recent crystal structure of the MHV six-helix bundle further clarifies that the extreme amino-terminal end of HR1 is not involved directly in the fusion core complex, as the interaction with HR2 is more central (68). Similar crystal structures are available for SARS-CoV and human CoV NL63 (57, 69, 76). While these models do not demonstrate involvement of the equivalent 948 and 949 residues for other CoVs in six-helix bundle formation, these positions may be influencing HR interactions in the context of virus. The coiled-coil structure, upon fusion, likely brings the amino-terminal end of HR1 and the PEP3 region in closer proximity to the transmembrane region, possibly providing an opportunity for the involvement of the PEP3-HR1 cluster of substitutions in facilitating or stabilizing the fusion core complex. Also revealed by the MHV crystal structure is that the linker region can be radically modified and still permit HR1-HR2 fusion core formation. This revelation complicates the interpretation of the influence of the 1120T and 1179A substitutions, as they appear to contribute to the host range phenotype as evidenced by the subtle difference in phenotype recovery between the S2 and PEP3/HR1 recombinants. Alternatively, the HR1 and PEP3 substitutions may not be involved in the formation of the six-helix bundle but are important in coordinating S1-S2 interactions and the fusion trigger. S structural data for the pre- and postfusion states are desperately needed to resolve this issue.

Of great interest is the location of the PEP3-HR1 substitutions when viewed in light of growing optimism for HR-based peptide inhibitors of viral fusion. The recent approval of the HR2-based HIV fusion inhibitor enfuvirtide (T20 or Fuzeon) for HIV treatment is just one example, but many others have been evaluated in vitro, including for SARS-CoV (8, 35, 39, 48, 63, 73). Another host range model system using the retrovirus avian sarcoma and leukosis virus subgroup A (ASLV A) passaged virus in the presence of a HR2-based inhibitor (1). Such passage readily selected peptide-resistant variants, several with substitutions in the amino-terminal portion of HR1. A subset of these variants was able to infect nonavian cells, including human cells, and displayed altered SU-TM (the S1-S2 equivalents, respectively, in retroviruses) stability. In those host range variants displaying the strongest replication in human cells, the responsible substitutions were preliminarily mapped to the interface between HR1 and HR2. Paralleling the MHV model, additional ASLV host range mutants were generated with the governing mutations mapping to SU (47). We are in the process of evaluating the sensitivity of V51 to an HR2-based peptide to understand whether the changes in HR1 of V51 are altering the fusion process at the six-helix bundle level. We presume that increased resistance to the HR2 peptide would indicate that the fusion core is affected, while no change in resistance suggests that the substitutions are involved in stabilizing S1-S2 or receptor interactions. The panel of viruses produced in the study by de Haan et al. was reportedly inhibited effectively with an HR2-based peptide (18), suggesting that those HR1 substitutions were involved in processes other than fusion core formation, perhaps associated with MHV/BHK usage of HS as a receptor in HeLa cells.

The loss of affinity for CEACAM1a based on changes in S2 was particularly interesting, as the substitutions in the RBD alone were not the predominant mediators of host range expansion. Recombinants harboring S1 from V51 could still initiate infection via CEACAM1a, as demonstrated by the S1 recombinant (Fig. 6A). The MHV/BHK variant displayed a similar phenotype, as it was less sensitive to soluble receptor neutralization but still capable of binding to CEACAM1a (53, 60). Particularly intriguing were the 3′ region and S2 recombinants. Both recombinants possess at a minimum the A59 RBD, yet they recovered less than 1% of the A59 titers on ST-CEACAM1a cells. While we do not know the CEACAM1a binding affinities of our recombinant panel, it appears that the substitutions outside the RBD modulate either CEACAM1a binding or S1-S2 interactions and prevent the entry of these recombinants and V51. In the context of the working MHV entry model, the V51 S1 subunit is clearly able to transfer the receptor binding signal to an A59-based S2, as demonstrated by the robust replication of the S1 recombinant, but the inverse situation is apparently not occurring normally, if at all. This result may indicate that the V51 S2 substitutions are altering S1-S2 or receptor interactions, the fusion trigger, and not HR1-HR2 interactions.

The convergence of phenotype between V51- and HR2-resistant ASLV isolates deserves attention. The common localization of mutations mediating host range to domains conserved in class I fusion proteins suggests that such proteins may have an inherent plasticity in the mechanism that could be exposed under the correct environmental conditions, such as fusion-specific inhibitory drugs. The selective pressure of the immune system may be the power in the system limiting evolution in the fusion mechanism at present. This power would explain why changes thought to be responsible for SARS-CoV emergence occurred in the RBD, although this result has yet to be evaluated in the context of virus infection. There are additional changes in SARS-CoV S, relative to earlier animal isolates, with unknown functions. Also, as Amberg et al. pointed out, the ASLV host range isolates were more sensitive to neutralizing antibodies and had a lower activation threshold necessary to induce SU conformational changes (1). We do not have enough data on S1-S2 stability or the sensitivity of V51 to neutralizing antibodies at present to make relevant comparisons with ASLV. It will be interesting to follow the development of the enfuvirtide story, as it brings together all the variables discussed here: an immunosuppressed environment, a class I fusion protein, and a fusion-inhibiting compound. While clear host range variants have yet to be described, this therapeutic intervention may allow evolution in the fusion mechanism to manifest itself as altered HIV tropism and force us to carefully evaluate HR2-based compounds as therapeutic options.

ACKNOWLEDGMENTS

We thank Boyd Yount and Kris Curtis for technical expertise and helpful discussions during the course of this project. We also thank Amy Sims for critical evaluation of the manuscript. This project was greatly supported by the UNC-Chapel Hill sequencing and primer synthesis core facilities.

This work was supported by National Institutes of Health (NIH) National Institute of Allergies and Infectious Diseases grant AI23946-15 and NIH Molecular Biology of Viral Diseases predoctoral training grant AI07419-13.

REFERENCES

1. **Amberg, S. M., R. C. Netter, G. Simmons, and P. Bates.** 2006. Expanded tropism and altered activation of a retroviral glycoprotein resistant to an entry inhibitor peptide. J. Virol. **80:**353–359.
2. **Baric, R. S., K. Fu, M. C. Schaad, and S. A. Stohlman.** 1990. Establishing a genetic recombination map for murine coronavirus strain A59 complementation groups. Virology **177:**646–656.
3. **Baric, R. S., E. Sullivan, L. Hensley, B. Yount, and W. Chen.** 1999. Persistent infection promotes cross-species transmissibility of mouse hepatitis virus. J. Virol. **73:**638–649.
4. **Baric, R. S., B. Yount, L. Hensley, S. A. Peel, and W. Chen.** 1997. Episodic evolution mediates interspecies transfer of a murine coronavirus. J. Virol. **71:**1946–1955.
5. **Beauchemin, N., T. Chen, G. Draber, G. Dveksler, P. Gold, S. Gray-Owen, F. Grunert, S. Hammarstrom, K. V. Holmes, A. Karlson, M. Kuroki, S. H. Lin, L. Lucka, S. M. Najjar, M. Neumaier, B. Obrink, J. E. Shively, K. M. Skubitz, C. P. Stanners, P. Thomas, J. A. Thompson, M. Virji, S. von Kleist, C. Wagener, S. Watt, and W. Zimmerman.** 1999. Redefined nomenclature for members of the carcinoembryonic antigen family. Exp. Cell Res. **252:** 243–249.
6. **Blau, D. M., C. Turbide, M. Tremblay, M. Olson, S. Letourneau, E. Michaliszyn, S. Jothy, K. V. Holmes, and N. Beauchemin.** 2001. Targeted disruption of the *Ceacam1* (*MHVR*) gene leads to reduced susceptibility of mice to mouse hepatitis virus infection. J. Virol. **75:**8173–8186.
7. **Bos, E. C., L. Heijnen, W. Luytjes, and W. J. Spaan.** 1995. Mutational analysis of the murine coronavirus spike protein: effect on cell-to-cell fusion. Virology **214:**453–463.
8. **Bosch, B. J., B. E. Martina, R. Van Der Zee, J. Lepault, B. J. Haijema, C. Versluis, A. J. Heck, R. De Groot, A. D. Osterhaus, and P. J. Rottier.** 2004. Severe acute respiratory syndrome coronavirus (SARS-CoV) infection inhibition using spike protein heptad repeat-derived peptides. Proc. Natl. Acad. Sci. USA **101:**8455–8460.
9. **Bosch, B. J., R. van der Zee, C. A. de Haan, and P. J. Rottier.** 2003. The coronavirus spike protein is a class I virus fusion protein: structural and functional characterization of the fusion core complex. J. Virol. **77:**8801–8811.
10. **Boyle, J. F., D. G. Weismiller, and K. V. Holmes.** 1987. Genetic resistance to mouse hepatitis virus correlates with absence of virus-binding activity on target tissues. J. Virol. **61:**185–189.
11. **Cabirac, G. F., K. F. Soike, J. Y. Zhang, K. Hoel, C. Butunoi, G. Y. Cai, S. Johnson, and R. S. Murray.** 1994. Entry of coronavirus into primate CNS following peripheral infection. Microb. Pathog. **16:**349–357.
12. **Chambers, P., C. R. Pringle, and A. J. Easton.** 1990. Heptad repeat sequences are located adjacent to hydrophobic regions in several types of virus fusion glycoproteins. J. Gen. Virol. **71:**3075–3080.
13. **Chen, D. S., M. Asanaka, F. S. Chen, J. E. Shively, and M. M. C. Lai.** 1997. Human carcinoembryonic antigen and biliary glycoprotein can serve as mouse hepatitis virus receptors. J. Virol. **71:**1688–1691.
14. **Colman, P. M., and M. C. Lawrence.** 2003. The structural biology of type I viral membrane fusion. Nat. Rev. Mol. Cell Biol. **4:**309–319.
15. **Compton, S. R., C. B. Stephensen, S. W. Snyder, D. G. Weismiller, and K. V. Holmes.** 1992. Coronavirus species specificity: murine coronavirus binds to a mouse-specific epitope on its carcinoembryonic antigen-related receptor glycoprotein. J. Virol. **66:**7420–7428.
16. **de Groot, R. J., W. Luytjes, M. C. Horzinek, B. A. van der Zeijst, W. J. Spaan, and J. A. Lenstra.** 1987. Evidence for a coiled-coil structure in the spike proteins of coronaviruses. J. Mol. Biol. **196:**963–966.
17. **de Haan, C. A., Z. Li, E. te Lintelo, B. J. Bosch, B. J. Haijema, and P. J. Rottier.** 2005. Murine coronavirus with an extended host range uses heparan sulfate as an entry receptor. J. Virol. **79:**14451–14456.
18. **de Haan, C. A., E. Te Lintelo, Z. Li, M. Raaben, T. Wurdinger, B. J. Bosch, and P. J. Rottier.** 2006. Cooperative involvement of the S1 and S2 subunits of the murine coronavirus spike protein in receptor binding and extended host range. J. Virol. **80:**10909–10918.
19. **Delmas, B., J. Gelfi, R. L'Haridon, L. K. Vogel, H. Sjostrom, O. Noren, and H. Laude.** 1992. Aminopeptidase N is a major receptor for the enteropathogenic coronavirus TGEV. Nature **357:**417–420.
20. **Dveksler, G. S., C. W. Dieffenbach, C. B. Cardellichio, K. McCuaig, M. N. Pensiero, G. S. Jiang, N. Beauchemin, and K. V. Holmes.** 1993. Several members of the mouse carcinoembryonic antigen-related glycoprotein family are functional receptors for the coronavirus mouse hepatitis virus-A59. J. Virol. **67:**1–8.
21. **Dveksler, G. S., M. N. Pensiero, C. B. Cardellichio, R. K. Williams, G. S. Jiang, K. V. Holmes, and C. W. Dieffenbach.** 1991. Cloning of the mouse hepatitis virus (MHV) receptor: expression in human and hamster cell lines confers susceptibility to MHV. J. Virol. **65:**6881–6891.
22. **Dveksler, G. S., M. N. Pensiero, C. W. Dieffenbach, C. B. Cardellichio, A. A. Basile, P. E. Elia, and K. V. Holmes.** 1993. Mouse hepatitis virus strain A59 and blocking antireceptor monoclonal antibody bind to the N-terminal domain of cellular receptor. Proc. Natl. Acad. Sci. USA **90:**1716–1720.
23. **Eckert, D. M., and P. S. Kim.** 2001. Mechanisms of viral membrane fusion and its inhibition. Annu. Rev. Biochem. **70:**777–810.
24. **Fukushi, S., T. Mizutani, K. Sakai, M. Saijo, F. Taguchi, M. Yokoyama, I. Kurane, and S. Morikawa.** 2007. Amino acid substitutions in the S2 region enhance severe acute respiratory syndrome coronavirus infectivity in rat angiotensin-converting enzyme 2-expressing cells. J. Virol. **81:**10831–10834.
25. **Gallagher, T. M.** 1997. A role for naturally occurring variation of the murine coronavirus spike protein in stabilizing association with the cellular receptor. J. Virol. **71:**3129–3137.
26. **Gallagher, T. M., and M. J. Buchmeier.** 2001. Coronavirus spike proteins in viral entry and pathogenesis. Virology **279:**371–374.
27. **Grosse, B., and S. G. Siddell.** 1994. Single amino acid changes in the S2 subunit of the MHV surface glycoprotein confer resistance to neutralization by S1 subunit-specific monoclonal antibody. Virology **202:**814–824.
28. **Guan, Y., B. J. Zheng, Y. Q. He, X. L. Liu, Z. X. Zhuang, C. L. Cheung, S. W. Luo, P. H. Li, L. J. Zhang, Y. J. Guan, K. M. Butt, K. L. Wong, K. W. Chan, W. Lim, K. F. Shortridge, K. Y. Yuen, J. S. Peiris, and L. L. Poon.** 2003. Isolation and characterization of viruses related to the SARS coronavirus from animals in southern China. Science **302:**276–278.
29. **Hensley, L. E.** 1997. Molecular mechanisms of the cross-species transmission of mouse hepatitis virus. Ph.D. dissertation. University of North Carolina, Chapel Hill.
30. **Keele, B. F., F. Van Heuverswyn, Y. Li, E. Bailes, J. Takehisa, M. L. Santiago, F. Bibollet-Ruche, Y. Chen, L. V. Wain, F. Liegeois, S. Loul, E. M. Ngole, Y. Bienvenue, E. Delaporte, J. F. Y. Brookfield, P. M. Sharp, G. M. Shaw, M. Peeters, and B. H. Hahn.** 2006. Chimpanzee reservoirs of pandemic and nonpandemic HIV-1. Science **313:**523–526.
31. **Klimstra, W. B., K. D. Ryman, and R. E. Johnston.** 1998. Adaptation of Sindbis virus to BHK cells selects for use of heparan sulfate as an attachment receptor. J. Virol. **72:**7357–7366.
32. **Koetters, P. J., L. Hassanieh, S. A. Stohlman, T. Gallagher, and M. M. Lai.** 1999. Mouse hepatitis virus strain JHM infects a human hepatocellular carcinoma cell line. Virology **264:**398–409.
33. **Kubo, H., Y. K. Yamada, and F. Taguchi.** 1994. Localization of neutralizing epitopes and the receptor-binding site within the amino-terminal 330 amino acids of the murine coronavirus spike protein. J. Virol. **68:**5403–5410.
34. **Kuo, L., G. J. Godeke, M. J. Raamsman, P. S. Masters, and P. J. Rottier.** 2000. Retargeting of coronavirus by substitution of the spike glycoprotein ectodomain: crossing the host cell species barrier. J. Virol. **74:**1393–1406.
35. **Lambert, D. M., S. Barney, A. L. Lambert, K. Guthrie, R. Medinas, D. E. Davis, T. Bucy, J. Erickson, G. Merutka, and S. R. Petteway, Jr.** 1996. Peptides from conserved regions of paramyxovirus fusion (F) proteins are potent inhibitors of viral fusion. Proc. Natl. Acad. Sci. USA **93:**2186–2191.
36. **Lau, S. K., P. C. Woo, K. S. Li, Y. Huang, H. W. Tsoi, B. H. Wong, S. S. Wong, S. Y. Leung, K. H. Chan, and K. Y. Yuen.** 2005. Severe acute respiratory syndrome coronavirus-like virus in Chinese horseshoe bats. Proc. Natl. Acad. Sci. USA **102:**14040–14045.
37. **Li, W., Z. Shi, M. Yu, W. Ren, C. Smith, J. H. Epstein, H. Wang, G. Crameri, Z. Hu, H. Zhang, J. Zhang, J. McEachern, H. Field, P. Daszak, B. T. Eaton, S. Zhang, and L. F. Wang.** 2005. Bats are natural reservoirs of SARS-like coronaviruses. Science **310:**676–679.
38. **Li, W., S. K. Wong, F. Li, J. H. Kuhn, I. C. Huang, H. Choe, and M. Farzan.** 2006. Animal origins of the severe acute respiratory syndrome coronavirus: insight from ACE2-S-protein interactions. J. Virol. **80:**4211–4219.
39. **Liu, S., G. Xiao, Y. Chen, Y. He, J. Niu, C. R. Escalante, H. Xiong, J. Farmar, A. K. Debnath, P. Tien, and S. Jiang.** 2004. Interaction between heptad repeat 1 and 2 regions in spike protein of SARS-associated coronavirus: implications for virus fusogenic mechanism and identification of fusion inhibitors. Lancet **363:**938–947.
40. **Luo, Z., A. M. Matthews, and S. R. Weiss.** 1999. Amino acid substitutions within the leucine zipper domain of the murine coronavirus spike protein cause defects in oligomerization and the ability to induce cell-to-cell fusion. J. Virol. **73:**8152–8159.
41. **Luo, Z., and S. R. Weiss.** 1998. Roles in cell-to-cell fusion of two conserved hydrophobic regions in the murine coronavirus spike protein. Virology **244:** 483–494.
42. **Luytjes, W., L. S. Sturman, P. J. Bredenbeek, J. Charite, B. A. van der Zeijst, M. C. Horzinek, and W. J. Spaan.** 1987. Primary structure of the glycoprotein E2 of coronavirus MHV-A59 and identification of the trypsin cleavage site. Virology **161:**479–487.
43. **Matsuyama, S., and F. Taguchi.** 2002. Communication between S1N330 and

a region in S2 of murine coronavirus spike protein is important for virus entry into cells expressing CEACAM1b receptor. Virology **295:**160–171.
44. **Matsuyama, S., and F. Taguchi.** 2002. Receptor-induced conformational changes of murine coronavirus spike protein. J. Virol. **76:**11819–11826.
45. **Murray, R. S., G. Y. Cai, K. Hoel, J. Y. Zhang, K. F. Soike, and G. F. Cabirac.** 1992. Coronavirus infects and causes demyelination in primate central nervous system. Virology **188:**274–284.
46. **Nédellec, P., G. S. Dveksler, E. Daniels, C. Turbide, B. Chow, A. A. Basile, K. V. Holmes, and N. Beauchemin.** 1994. Bgp2, a new member of the carcinoembryonic antigen-related gene family, encodes an alternative receptor for mouse hepatitis virus. J. Virol. **68:**4525–4537.
47. **Rainey, G. J. A., A. Natonson, L. F. Maxfield, and J. M. Coffing.** 2003. Mechanisms of avian retroviral host range expansion. J. Virol. **77:**6709–6719.
48. **Rapaport, D., M. Ovadia, and Y. Shai.** 1995. A synthetic peptide corresponding to a conserved heptad repeat domain is a potent inhibitor of Sendai virus-cell fusion: an emerging similarity with functional domains of other viruses. EMBO J. **14:**5524–5531.
49. **Rottier, P., K. Nakamura, P. Schellen, H. Volders, and B. J. Haijema.** 2005. Acquisition of macrophage tropism during the pathogenesis of feline infectious peritonitis is determined by mutations in the feline coronavirus spike protein. J. Virol. **79:**14122–14130.
50. **Ryman, K. D., W. B. Klimstra, and R. E. Johnston.** 2004. Attenuation of Sindbis virus variants incorporating uncleaved PE2 glycoprotein is correlated with attachment to cell-surface heparan sulfate. Virology **322:**1–12.
51. **Saeki, K., N. Ohtsuka, and F. Taguchi.** 1997. Identification of spike protein residues of murine coronavirus responsible for receptor-binding activity by use of soluble receptor-resistant mutants. J. Virol. **71:**9024–9031.
52. **Schickli, J. H., L. B. Thackray, S. G. Sawicki, and K. V. Holmes.** 2004. The N-terminal region of the murine coronavirus spike glycoprotein is associated with the extended host range of viruses from persistently infected murine cells. J. Virol. **78:**9073–9083.
53. **Schickli, J. H., B. D. Zelus, D. E. Wentworth, S. G. Sawicki, and K. V. Holmes.** 1997. The murine coronavirus mouse hepatitis virus strain A59 from persistently infected murine cells exhibits an extended host range. J. Virol. **71:**9499–9507.
54. **Singh, M., B. Berger, and P. S. Kim.** 1999. LearnCoil-VMF: computational evidence for coiled-coil-like motifs in many viral membrane-fusion proteins. J. Mol. Biol. **290:**1031–1041.
55. **Smith, A. L., C. B. Cardellichio, D. F. Winograd, M. S. de Souza, S. W. Barthold, and K. V. Holmes.** 1991. Monoclonal antibody to the receptor for murine coronavirus MHV-A59 inhibits viral replication in vivo. J. Infect. Dis. **163:**879–882.
56. **Sturman, L. S., C. S. Ricard, and K. V. Holmes.** 1990. Conformational change of the coronavirus peplomer glycoprotein at pH 8.0 and 37 degrees C correlates with virus aggregation and virus-induced cell fusion. J. Virol. **64:**3042–3050.
57. **Supekar, V. M., C. Bruckmann, P. Ingallinella, E. Bianchi, A. Pessi, and A. Carfi.** 2004. Structure of a proteolytically resistant core from the severe acute respiratory syndrome coronavirus S2 fusion protein. Proc. Natl. Acad. Sci. USA **101:**17958–17963.
58. **Taguchi, F.** 1995. The S2 subunit of the murine coronavirus spike protein is not involved in receptor binding. J. Virol. **69:**7260–7263.
59. **Taylor, L. H., S. M. Latham, and M. E. Woolhouse.** 2001. Risk factors for human disease emergence. Philos. Trans. R. Soc. Lond. B **356:**983–989.
60. **Thackray, L. B., and K. V. Holmes.** 2004. Amino acid substitutions and an insertion in the spike glycoprotein extend the host range of the murine coronavirus MHV-A59. Virology **324:**510–524.
61. **Tresnan, D. B., R. Levis, and K. V. Holmes.** 1996. Feline aminopeptidase N serves as a receptor for feline, canine, porcine, and human coronaviruses in serogroup I. J. Virol. **70:**8669–8674.
62. **Tsai, J. C., B. D. Zelus, K. V. Holmes, and S. R. Weiss.** 2003. The N-terminal domain of the murine coronavirus spike glycoprotein determines the CEACAM1 receptor specificity of the virus strain. J. Virol. **77:**841–850.
63. **Watanabe, S., A. Takada, T. Watanabe, H. Ito, H. Kida, and Y. Kawaoka.** 2000. Functional importance of the coiled-coil of the Ebola virus glycoprotein. J. Virol. **74:**10194–10201.
64. **Weismiller, D. G., L. S. Sturman, M. J. Buchmeier, J. O. Fleming, and K. V. Holmes.** 1990. Monoclonal antibodies to the peplomer glycoprotein of coronavirus mouse hepatitis virus identify two subunits and detect a conformational change in the subunit released under mild alkaline conditions. J. Virol. **64:**3051–3055.
65. **Woolhouse, M. E.** 2002. Population biology of emerging and re-emerging pathogens. Trends Microbiol. **10:**S3–S7.
66. **Woolhouse, M. E., and S. Gowtage-Sequeria.** 2005. Host range and emerging and reemerging pathogens. Emerg. Infect. Dis. **11:**1842–1847.
67. **Woolhouse, M. E., D. T. Haydon, and R. Antia.** 2005. Emerging pathogens: the epidemiology and evolution of species jumps. Trends Ecol. Evol. **20:**238–244.
68. **Xu, Y., Y. Liu, Z. Lou, L. Qin, X. Li, Z. Bai, H. Pang, P. Tien, G. F. Gao, and Z. Rao.** 2004. Structural basis for coronavirus-mediated membrane fusion. Crystal structure of mouse hepatitis virus spike protein fusion core. J. Biol. Chem. **279:**30514–30522.
69. **Xu, Y., Z. Lou, Y. Liu, H. Pang, P. Tien, G. Gao, and Z. Rao.** 2004. Crystal structure of severe acute respiratory syndrome coronavirus spike protein fusion core. J. Biol. Chem. **279:**49414–49419.
70. **Yeager, C. L., R. A. Ashmun, R. K. Williams, C. B. Cardellichio, L. H. Shapiro, A. T. Look, and K. V. Holmes.** 1992. Human aminopeptidase N is a receptor for human coronavirus 229E. Nature **357:**420–422.
71. **Yokomori, K., and M. M. C. Lai.** 1992. Mouse hepatitis virus utilizes two carcinoembryonic antigens as alternative receptors. J. Virol. **66:**6194–6199.
72. **Yount, B., M. R. Denison, S. R. Weiss, and R. S. Baric.** 2002. Systematic assembly of a full-length infectious cDNA of mouse hepatitis virus strain A59. J. Virol. **76:**11065–11078.
73. **Yuan, K., L. Yi, J. Chen, X. Qu, T. Qing, X. Rao, P. Jiang, J. Hu, Z. Xiong, Y. Nie, X. Shi, W. Wang, C. Ling, X. Yin, K. Fan, L. Lai, M. Ding, and H. Deng.** 2004. Suppression of SARS-CoV entry by peptides corresponding to heptad regions on spike glycoprotein. Biochem. Biophys. Res. Commun. **319:**746–752.
74. **Zelus, B. D., J. H. Schickli, D. M. Blau, S. R. Weiss, and K. V. Holmes.** 2003. Conformational changes in the spike glycoprotein of murine coronavirus are induced at 37°C either by soluble murine CEACAM1 receptors or by pH 8. J. Virol. **77:**830–840.
75. **Zhang, C., J. Wei, and S. He.** 2006. Adaptive evolution of the spike gene of SARS coronavirus: changes in positively selected sites in different epidemic groups. BMC Microbiol. **6:**88.
76. **Zheng, Q., Y. Deng, J. Liu, L. van der Hoek, B. Berkhout, and M. Lu.** 2006. Core structure of S2 from the human coronavirus NL63 spike glycoprotein. Biochemistry **45:**15205–15215.